Quantum droplets with particle imbalance in one-dimensional optical lattices

Jofre Vallès Muns

Supervised by: Ivan Morera[1,2] and Bruno Juliá-Díaz[1,2]

[1]Departament de Física Quàntica i Astrofísica, Universitat de Barcelona
[2]Institut de Ciències del Cosmos (ICCUB), Universitat de Barcelona

11 July 2022

We study the effect of particle imbalance in quantum droplets formed by a binary bosonic mixture in a one-dimensional optical lattice. In this situation not all bosons are paired and we encounter an interplay between bound states and individual atoms that leads to intriguing phenomena. For small imbalances, quantum droplets are able to support a finite difference in densities, thus showing an effective magnetization. As the imbalance increases, a critical point is reached at which the droplets expels the excess of particles and the magnetization is locked in the bulk. We study the effects of the imbalance from both the few- and many-body perspective and we are able to extrapolate our results to the thermodynamic limit.

Keywords: Quantum Droplets, Quantum Gases, Particle-imbalanced bosonic mixtures

Jofre Vallès Muns: jofrevalles@ub.edu

Acknowledgements

We want to thank Arnau Rios for facilitating us the access into a computer cluster, in which we did part of the computations.

I would like to thank Ivan Morera for his continuous guidance and immense help not only for this thesis, but also over the last months. I also wish to thank Bruno Juliá-Díaz for his constant assistance and help. Thank you both for making this work a very pleasing and rewarding experience.

Finally, I would also like to thank my family and friends for their generous support and kindness during this thesis, *gràcies de tot cor*.

Contents

1 Introduction

Recently a whole new class of ultra-dilute quantum droplets has been produced in ultracold atomic laboratories with dipolar bosonic atoms [FBKS+16, SWB+16, CBP+16] and bosonic mixtures [CTS+18, CCS+18, SFM+18, DBP+19]. These quantum droplets originate from a compensation between mean-field and quantum fluctuations [Pet15] and consist of a new type of liquids, which their densities can be eight orders of magnitude more dilute than liquid helium droplets [BSH+20], the other only known quantum liquid at zero temperature [BGH+06].

Ultracold atomic systems can be trapped in optical lattice potentials. These ones create a periodic potential structure where atoms can interact on-site and tunnel between sites. Interacting spinless bosons in a high optical lattice at zero temperature are described by the Bose-Hubbard model [Kru16], a model which has been deeply studied in recent years [LSA12]. Ultracold setups like this offer a high control over the system and make them perfect platforms for testing quantum properties in a controlled manner.

In particular, ultracold atomic systems can be trapped in a potential that limits its movement to only one-dimension [SGM19]. This is then known as a one-dimensional system. Quantum droplets in one-dimensional systems show interesting results compared with the 3D case. In this situation the mean-field contribution is on average repulsive and predicts a stable gas and it is the quantum fluctuations from the beyond-mean-field term that result in an effective attraction that are able to liquefy the system [PA16]. In addition, in one-dimensional systems the stability is increased due to the suppression of three-body losses [TOH+04].

Quantum droplets made of bosonic binary mixtures on a one-dimensional lattice have been studied in the particle-balanced situation [MAPJD20, MAPJD21], where the number of atoms of both species is equal. In this thesis we go one step further and study the effect of particle imbalance on these quantum droplets. First, we describe the model and the numerical method we use in section 2, as well as a description of the situation in the balanced case. Then in section 3, we characterize the effects of particle imbalance in the few-body limit. We observe a rich collection of bound states. We characterize them by computing the respective binding energies and correlation functions. The effects of particle imbalance in the many-body limit are studied in section 4. In this limit we find that quantum droplets are able to support a finite difference in the density of both species, and thus gain an effective magnetization. This happens until a critical imbalance above which they expel particles outside the droplet and the magnetization is locked. Furthermore, we are able to obtain a prediction of the magnetization in the low particle imbalance and large interaction strength regime. To do this we consider the density profile of the majority component as the sum of the density of a Tonks–Girardeau gas of excess particles with the density of the minority component in the mixture. To characterize the coherence properties of particle-imbalanced quantum droplets we compute the one-body density matrix. Finally, we show that our results of the magnetization obey a simple scaling relation for different total number of particles. To understand the expulsion mechanism we study the thermodynamic limit and compute the chemical potential of the majority component. This allows us to predict the expulsion point.

2 Model

We study a binary mixture of bosonic atoms with short-range interactions loaded in a deep one-dimensional optical lattice at zero temperature. We assume the system can be described to a good approximation by the two-component Bose-Hubbard Hamiltonian [LSA12],

$$\hat{H} = -t \sum_i \sum_{\alpha=A,B} \left(\hat{b}^\dagger_{i,\alpha} \hat{b}_{i+1,\alpha} + \text{h.c.} \right) + \frac{U}{2} \sum_i \sum_{\alpha=A,B} \hat{n}_{i,\alpha}(\hat{n}_{i,\alpha} - 1) + U_{AB} \sum_i \hat{n}_{i,A} \hat{n}_{i,B} \,, \quad (1)$$

where $\hat{b}_{i,\alpha}$ ($\hat{b}^\dagger_{i,\alpha}$) are the annihilation (creation) bosonic operators at site $i = 1, \ldots, L$ for species $\alpha = A, B$; and $\hat{n}_{i,\alpha}$ are their corresponding number operators.

In this work we focus on the situation of equal tunneling strength for both species, $t > 0$, and an equal repulsive intra-species interaction strength, $U > 0$. In the following we use t as the energy scale and keep it fixed throughout the entire work. We study the case of attractive inter-species interaction, $U_{AB} < 0$, and we introduce the dimensionless ratio $r = 1 + U_{AB}/U$.

2.1 Density Matrix Renormalization Group

To compute the ground state of this system we use the Density Matrix Renormalization Group (DMRG) algorithm. DMRG is a very efficient method to study one-dimensional systems with short-range entanglement structure. This method was initially proposed as a numerical renormalization technique [Whi92].

In recent years, Tensor Network (TN) based methods have been widely used to study many-body quantum systems. The main idea behind TN methods is to describe the wave function of the system with a network of interconnected tensors [Or4]. It can be seen that TNs offer very efficient descriptions of many-body states and take advantage of the locality of entanglement in the system. Matrix Product States (MPS) are a particular case of TNs which describe one-dimensional systems decomposing the wave function ψ into products of matrices,

$$|\psi\rangle = \sum_{n_1,\ldots,n_L} T^{[1]n_1}_{\alpha_1\alpha_2} T^{[2]n_2}_{\alpha_2\alpha_3} \ldots T^{[N]n_L}_{\alpha_L\alpha_{L+1}} |n_1, \ldots, n_L\rangle \,, \quad (2)$$

where L is the number of sites, there are $\dim(n_i)$ matrices $T^{[i]n_i}$ of dimension $\chi_i \times \chi_{i+1}$ for each site i, and we are using Einstein notation, so we sum over the repeated indices. The superscript $[i]$ denotes the set of matrices in this particular i site, the subscripts $\alpha_i\alpha_{i+1}$ are called bond indices and the superscript n_i is called a physical index, since it refers to the site i in the lattice. We name the bond dimension χ the maximum value that we enable for the dimension of these matrices.

The main idea behind TNs is that in order to represent a many-body system we do not need to know the full Hilbert space of the problem, instead we can limit to only a small part of it which follows an area law for the entanglement entropy [Or4]. This means that the entanglement entropy of these states grows proportionally with the size of the boundary between partitions and not with its volume, as would be expected for an arbitrary many-body state. It has been proved that low-energy states of gapped, local, frustration-free Hamiltonians in one-dimension fulfill an area law [Has07]. This makes TNs very good methods to study one-dimensional systems with high efficiency. Nowadays, DMRG has been reinterpreted as a variational approach to optimize the respective MPS [Sch11].

In the DMRG computations used in this work we put a cutoff on the maximum number of bosons of each species per site of $M = 4$ for simulations with sufficiently large interaction

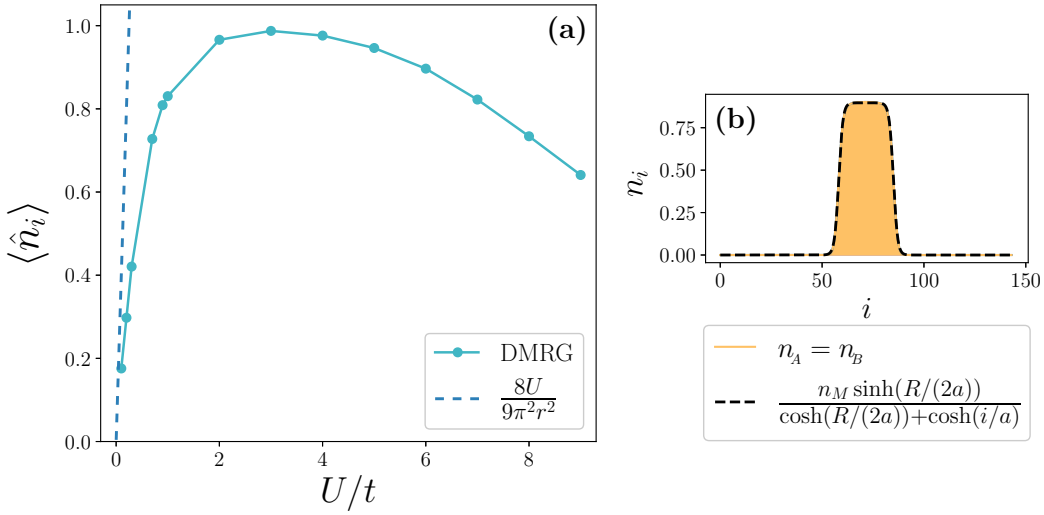

Figure 1: (a) Averaged density in the bulk of the droplet as a function of the interaction strength U/t for $r = 0.15$, maximum number of bosons per site $M = 6$ and different L, ensuring that the droplets fit inside the lattice. (b) Typical density profile of a droplet compared with the corresponding fit using eq. (3). The droplet in panel (b) is obtained for $U/t = 4$, $L = 144$ and $N_A = N_B = 24$.

strength U/t. This gives a dimension of the local Hilbert space of $d = (M+1)^2 = 25$. For systems with open boundary conditions the maximum bond dimension is set to $\chi = 256$ for quantitative results of the density and energy of the system and $\chi = 2048$ when we study correlation functions. For systems with periodic boundary conditions we use $\chi = 512$ to extract the energy of the system. This choice of the bond dimension χ and the value M for different quantities obtained in this work is discussed in Appendix A.

2.2 Particle-balanced situation

In a bosonic binary mixture in a one-dimensional lattice at zero temperature, quantum droplets in the particle-balanced situation are able to exist for any strength of repulsive intra-species interactions provided they are compensated by comparable attractive inter-species interactions [MAPJD20]. In the following subsection, we give a brief review of the key aspects of these droplets in this particle-balanced situation, that is when the number of atoms of both species is equal $N_A = N_B$.

2.2.1 Density profile

Our numerical approach with DMRG allows us to obtain the density profile of the ground state. This one gives us important insight on to the phases of the object and can be employed to detect the presence of a quantum droplet. Moreover the profile of a droplet can be fit to a symmetrized Fermi function [SM98],

$$n_i = \frac{n_M \sinh(R/(2a))}{\cosh(R/(2a)) + \cosh(i/a)}\,, \tag{3}$$

where R is the size of the droplet, a the typical length scale of the meniscus and n_M is also a free parameter. In Fig. 1(b) we show a fit to the density profile of a droplet using this function.

In Fig. 1(a) we show the evolution of the averaged central density in the bulk of the droplet as a function of the interaction strength U/t and fixed r. For low values of the

interaction strength U/t the density tends to the beyond-mean-field (BMF) prediction of the equilibrium density in the continuum, $n_i = 8U/9\pi^2 r^2$ [AM18]. This is expected since for low U/t the effects of the lattice are more suppressed. Thus for $U/t \to 0$ we expect to recover BMF results. For large U/t the one-dimensional lattice is able to stabilize the density of the droplet and stop the rapidly-growing value of the mean-field prediction. This feature shows one of the advantages of the lattice, where lower values in the equilibrium density imply lower three-body losses. Droplets with small values of the interaction strength U/t are hard to compute since its equilibrium densities are very low and thus large lattices are needed to fit the entire droplet. This same numerical problem occurs for large U/t where droplets disappear. For $U/t = 2/r$ the droplet is expected to vanish into a gas [MAPJD21]. This is seen in the density profile since the droplet grows its size and eventually disappears the exponential decay in the meniscus.

The prediction of $U/t = 2/r$ was obtained identifying the transition between attraction and repulsion in the effective interaction between dimers. Dimers are bound states of one A and one B particle. This result suggests that important information of quantum droplets can be captured from the few-body limit. We can identify bound states and we can study the droplet as interactions between these.

2.2.2 Phases in the droplet

Quantum droplets show superfluid properties in one-dimensional optical lattices. Moreover they can be classified in two different phases: two-atomic superfluids (2SF) and pair superfluids (PSF). A 2SF state is characterized by a quasi-long range phase coherence in both species. This can be seen in both one- ($\langle \hat{b}_{i,\alpha} \hat{b}^\dagger_{j,\alpha} \rangle$) and two-body ($\langle \hat{b}_{i,A} \hat{b}_{i,B} \hat{b}^\dagger_{j,A} \hat{b}^\dagger_{j,B} \rangle$) correlation functions as a power-law decay behavior. On the other hand, the PSF state is characterized by the formation of pairs of atoms which show long-range phase coherence [HMD+09]. In our system, these pairs are two atoms of different species, i.e., dimers. Therefore in the PSF the correlation function of pairs decays with a power-law. However, the correlations of bosons of the same species decay exponentially [HMD+09]. This enables to identify the transition between these two regimes, and it can be observed for a fixed r and different interaction strengths U/t. Droplets are able to exist until a critical U/t above which they vanish into a gas and a Mott-insulator phase can be found if the filling factor N/L is integer, where $N = N_A = N_B$.

3 Particle imbalance in few-body systems

Now we turn our attention to the central topic of this work, which is when the number of particles in both species differ. Motivated from the fact that in the particle-balanced situation the few-particle case offers great insight into the problem, we first consider the effect of particle imbalance in few-body systems. To understand the internal structure of the solution, we will perform calculations using different particle numbers to understand the presence of composite bound states, i.e., dimers, trimers, ...

3.1 Four-particle case

The minimal system we consider consists of four bosons $N_A + N_B = 4$. In the balanced situation ($N_A = N_B = 2$) for large enough U we expect the system to be dimerized [MAPJD21]. In this regime an effective interaction between dimers emerges. In order to rule out the presence of trimers in the particle-balanced situation we compute the respective binding energies. In Fig. 2 we report the energy of two dimers AB and a trimer AAB with a free particle B. The sum of the energy of two dimers is always lower than the sum of the energy of a trimer and the energy of a free particle. Therefore we conclude that in the particle-balanced case in dilute region the dimer is always more stable than other larger bound states, since the ground state of the system always binds with the lowest energy state.

3.2 Bound states with particle imbalance

When particle imbalance is present in the system the formation of larger bound states is enhanced. This leads to different phenomena than in the balanced case. In this scenario dimers are not necessarily the most stable bound states. Thus other larger bound states can be created. We show that the type of bound state depends on the interaction strength U/t and thus a transition between different bound states can be observed for a fixed r and

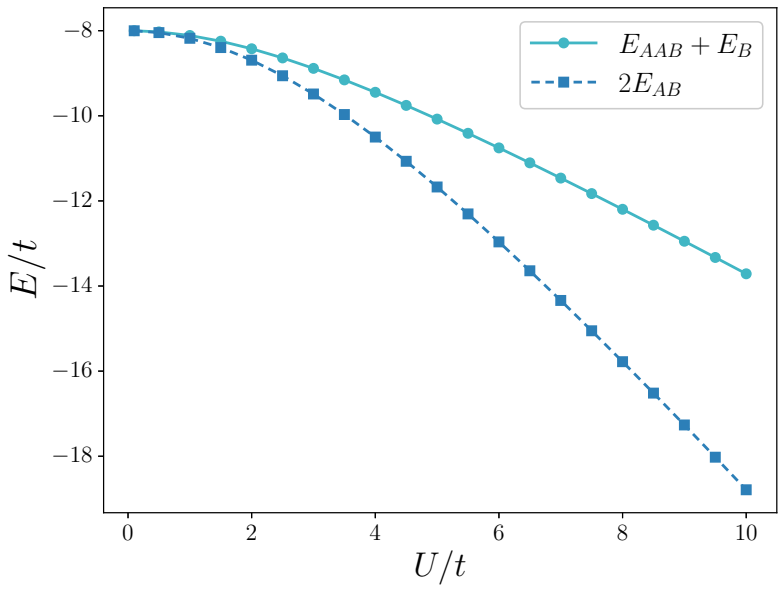

Figure 2: Energy as a function of the interaction strength U/t for $r = 0.15$ and a lattice of size $L = 200$. Both curves are obtained for $N_A = N_B = 2$. Circles represent the energy of a trimer AAB and a free B particle and squares the energy of two dimers AB.

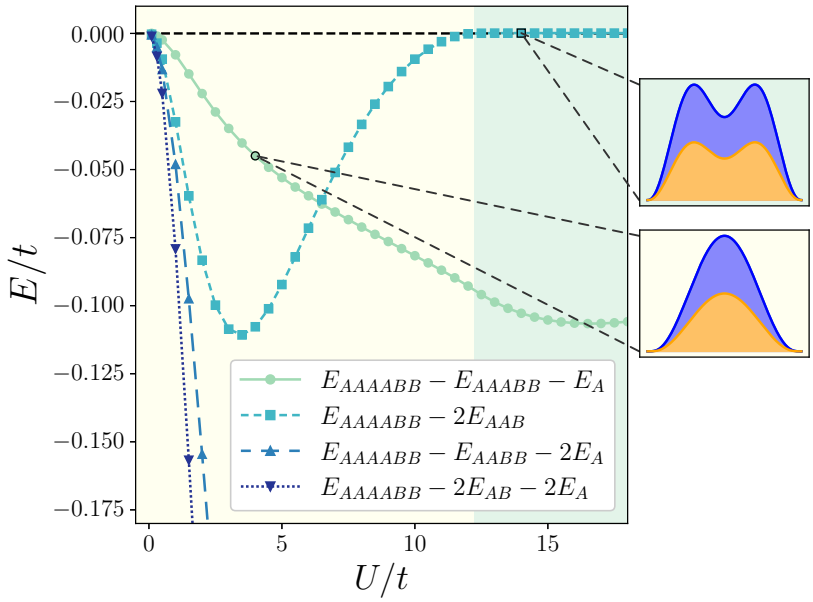

Figure 3: In the main plot, we show the binding energies of the hexamer state $(N_A = 4, N_B = 2)$ as a function of the interaction strength U/t for $r = 0.15$ and $L = 200$. The green zone in the background is the region where two trimers are not bound together, this is identified when its binding energy turns zero. On the right, we show the density profiles of the hexamer state in the corresponding interaction strength U/t marked with grey dashed lines.

a fixed N_A and N_B. This can be seen in Fig. 3, where we show different decomposition channels for the hexamer state $AAAABB$. The most likely decomposition channel is identified with the one which its binding energy is closer to zero. When the value of the binding energy is zero the system fully decomposes into the respectively bound states. In this figure it can be seen that for $U/t \lesssim 6.5$ the system binds into a pentamer $AAABB$ and an atom A and for $U/t \gtrsim 6.5$ the system binds into two trimers AAB. We can also notice that in contrast to the particle-balanced case, in this the system never dimerizes and instead the trimer state plays a similar role as the dimer. In Fig. 4 we show the binding energies for two-dimer and two-trimer states. This similarity between dimer and trimer (and other bound states for different interactions and particle imbalances) may indicate that quantum droplets can be created when there is this type of imbalance in the system, as we will further see in section 4. In the continuum in a two-dimensional system it has been seen that this similarity in the binding energies does not happen and instead the dimer and trimer bind in different interaction strengths [GAB+20].

From $U/t \gtrsim 6.5$ the two trimers are bound until $U/t \gtrsim 12$, where in Fig. 3 we observe that the binding energy of the hexamer with two trimers becomes zero. This transition is also reflected in the density functions as a physical separation of the two trimers. With this variety of bound states in the few-body case we expect a wide range of large bound states in the many-body that can change for different interaction strengths U/t. This will have strong consequences in the many-body properties of the system.

We now study the effect of changing the number of B particles while keeping fixed the number of A particles. We consider the balanced case of $N_A = N_B = 4$ and we remove B particles. We study the binding energies and the correlation functions which give us information on the different bound states in the system. For $N_B \geq 2$ the B particles are able to be bound with the other 4 A particles. However, for $N_B = 1$ the B particle alone is not able to bind the rest and instead creates a trimer AAB and two A particles are

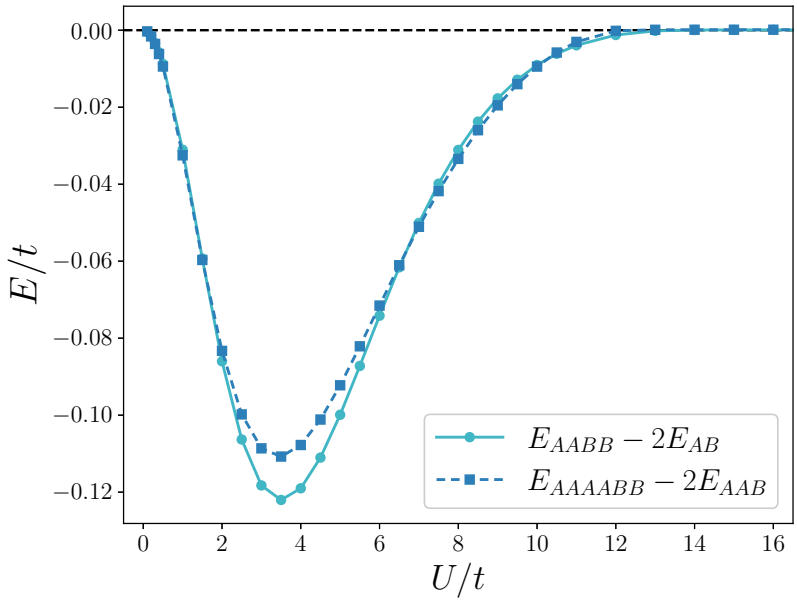

Figure 4: Binding energies as a function of the interaction strength U/t for $r = 0.15$ and $L = 200$. In circles and squares, the binding energy of the tetramer with two dimers AB and the hexamer with two trimers AAB, respectively.

left outside. We thus say that these two A particles are expelled from the large bound state, the trimer. This can be seen in Fig. 5(a) with the main binding energies, that is we identify which binding energy is closer to zero for each of these states. Thus we conclude that different bound states appear for different imbalances. In addition, in Fig. 5(b) we show that when there is no particle expelled, the correlation functions $\langle \hat{n}_i^A \, \hat{n}_j^A \rangle$ exhibit the typical exponential decay associated to bound states [SC95]. However, when there are particles expelled that are not bound the correlation function shows instead a different behavior: it first decays exponentially for small values of $|i - j|$ and then shows saturation, see Fig. 5(c).

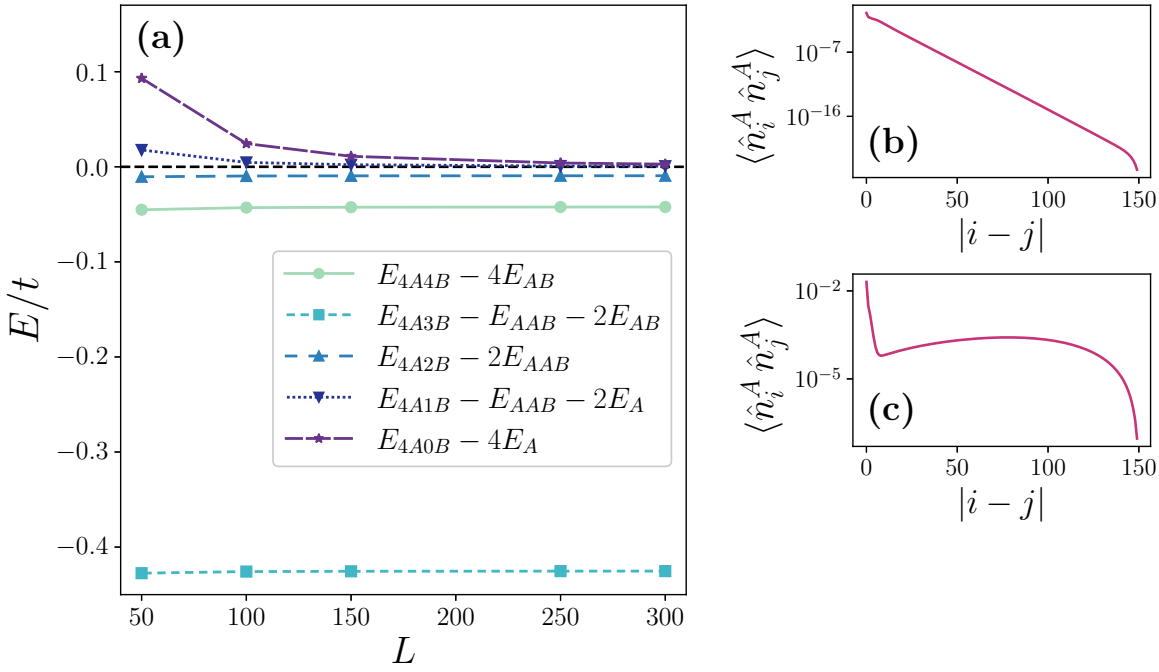

Figure 5: (a) Main decomposition binding energies as a function of the lattice size L. In both panels (b) and (c), the correlator $\langle \hat{n}_i^A \hat{n}_j^A \rangle$ with i fixed in the middle of the lattice and j scans from $j = i$ to the end of the lattice. In panel (b) the correlator is computed for $N_A = 4, N_B = 2$ and in (c) for $N_A = 4, N_B = 1$. All three panels are obtained for $U/t = 8$ and $r = 0.15$ and both panels (b) and (c) are obtained for $L = 300$.

4 Ground state properties in the particle-imbalanced situation

In the previous section we have shown that particle imbalance plays a relevant role in the few-body case. An important feature of DMRG techniques is that they can be used for fairly large particle numbers and system sizes, thus allowing us to study the transition from the few-body to the many-body regime. The main goal here is to describe the ground state properties in particle-imbalanced many-body systems. In particular, we want to find whether a given droplet solution in the balanced case is robust when we introduce a certain amount of this imbalance.

In the following, we quantify the particle imbalance in the system by means of the dimensionless variable $z = (N_A - N_B)/(N_A + N_B)$, where N_A and N_B are the total number of particles for the species A and B, respectively.

4.1 Particle-imbalanced quantum droplets

We study the effect of particle imbalance in quantum droplets. Beyond-mean-field studies of these droplets predict that excitations associated with particle imbalance are highly energetic and above the particle expulsion threshold, leading to an effective evaporation into the balanced case [Pet15]. In contrast to the continuum case, here we show that strongly correlated droplets in one-dimensional optical lattices are robust against a certain amount of this imbalance. To characterize this effect over the quantum droplets we introduce the magnetization $m_{ab} = (\langle \hat{n}_A \rangle - \langle \hat{n}_B \rangle)/2$, where $\langle \hat{n}_A \rangle$ ($\langle \hat{n}_B \rangle$) is the averaged density in the bulk of the droplet for the species A (B). We obtain this value as,

$$\langle \hat{n}_\alpha \rangle = \sum_{i-R/2-4a}^{i+R+4a} \frac{n_{i,\alpha}}{R+8a}\,, \tag{4}$$

where R and a are obtained fitting the densities of the droplet with eq. (3) and i is its center of mass. In Fig. 6 we show the evolution of the magnetization as the particle imbalance z is increased. To obtain this imbalance, we fix the number of particles N_A and remove B particles. Therefore, for $z = 0$ we recover the results of the balanced case and for $z = 1$ there is only the species A left in the system. As the imbalance is increased we identify two distinct regions: for small z the droplet gains magnetization and is able to support particle imbalance in density and for large z the droplet locks the magnetization by expelling A particles outside the droplet. In this second region we observe a plateau in the magnetization. We name the critical imbalance above which the droplet expels particles as z^*. The two regions can be clearly identified in the density profiles, see insets in Fig. 6. In the density profile of a droplet that has expelled particles, we observe the formation of a gas outside it.

Another remarkable property of the magnetization is that, for sufficiently large interaction strength U/t, we find that this quantity is universal given an imbalance z for any number of particles. This is visible in Fig. 6, where we present the magnetization for different number of particles. The total density of the droplet $n = n_A + n_B$ also features the same universality, but this one has non-trivial dependence with the imbalance quantity z.

Particle expulsion outside the droplet resembles the phenomena found in the few-body regime detailed in section 3. When particle imbalance is increased the system decomposes into a region of large bound states and a region of non-bound A particles. The critical value of the imbalance can be understood as the point in which the B particles are not able to bind the all other A particles and thus they are expelled.

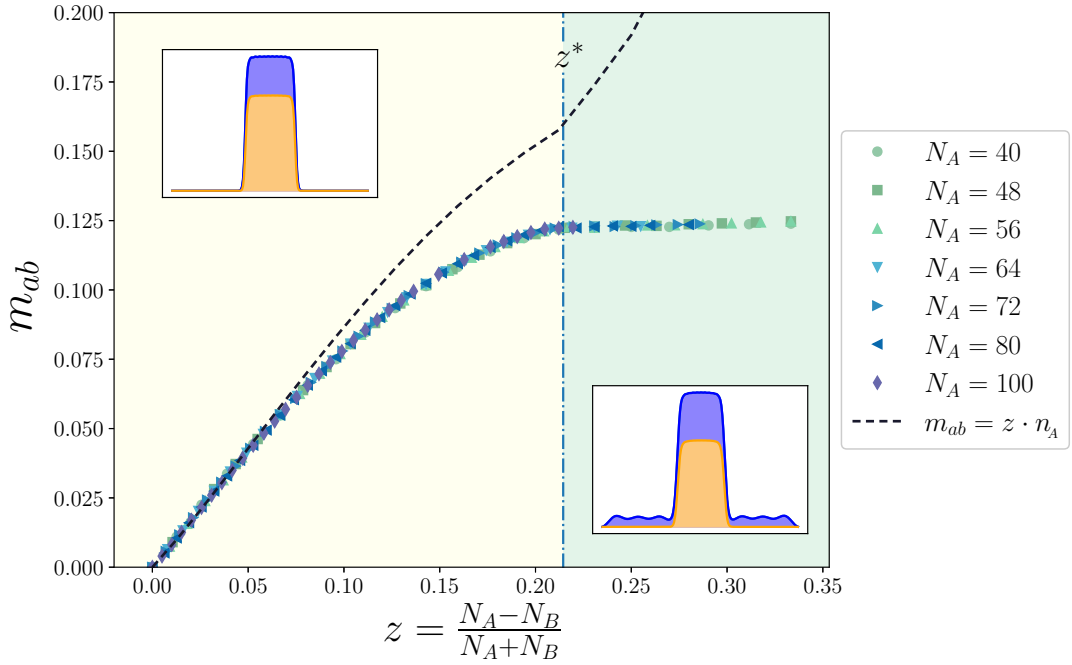

Figure 6: In the main plot, we show the magnetization m_{ab} (defined in the text) as a function of the imbalance quantity z. The vertical dashed-dotted line is the value of the critical imbalance z^*. The green region in the background shows where the system expels A particles outside the droplet. In the insets, we show the density profile of the component A and B in blue and orange, respectively, in the corresponding z region as a function of the lattice site. This figure was obtained for $U/t = 8$, $r = 0.15$ and $L = 200$. The droplets in the insets are obtained for $N_A = 40$.

The plateau in which the magnetization is locked after the critical z^* depends on the interactions between atoms (r, U). This plateau exists until another critical imbalance $\tilde{z}$ above which the system has not enough B particles and it is no longer self-bound. Thus the droplet disappears. $\tilde{z}$ is difficult to be studied quantitatively, since we find that the gas made of expelled particles creates an effective pressure into the droplet. This gas occupies the whole lattice except the part occupied by the droplet and therefore the value of this pressure depends vastly on the lattice size L.

4.2 Tonks–Girardeau gas of the excess particles

In the small particle imbalance and large interaction strength limit we numerically find that the density of the excess particles in A, $n_A(x) - n_B(x)$, resembles the density profile of a Tonks-Girardeau (TG) gas of $N_A - N_B$ particles in a box of size R given by the droplet size. The TG gas is a bosonic gas in one-dimension in which bosons are hard-core and thus are infinitely repulsive ($U \to \infty$). In this limit, bosons have such repulsion that they can be mapped to a system of spinless fermions [Gir60]. The density of the TG gas that we observe on top of the droplet is small. Therefore in this low-filling situation we expect the continuum description to work fairly well. This enables us to find an exact analytic solution. The single-particle wave function of a free particle in a one-dimensional box of size R is,

$$\psi_n(x) = \sqrt{\frac{2}{R}} \sin\left(\frac{n\pi}{R} x\right), \tag{5}$$

where $n = 1, 2, 3, \ldots$.

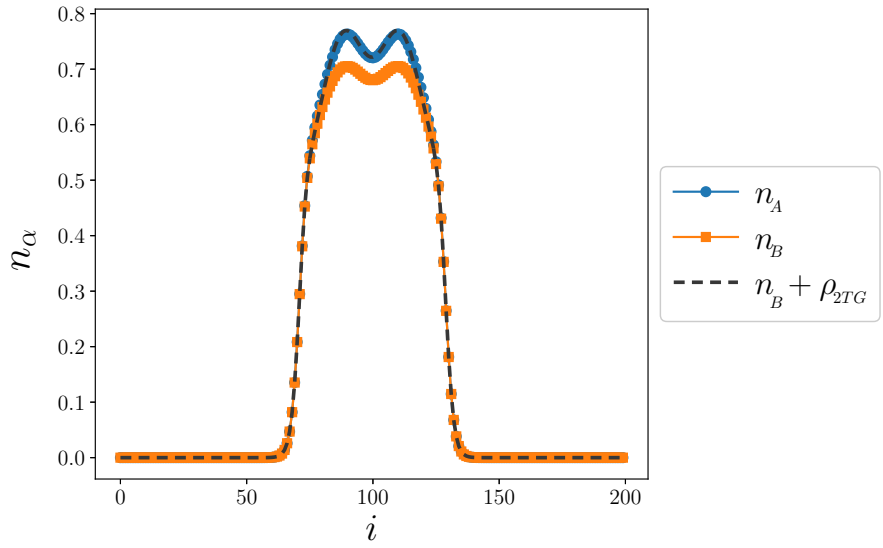

Figure 7: Density profile as a function of the lattice site i. The quantity ρ_{2TG} is the density of a TG gas of two particles in a one-dimensional box of size R, obtained from eq. (6). This droplet is obtained for $N_A = 40$, $N_B = 38$, $U/t = 10$, $r = 0.15$ and $L = 200$.

The fermionic many-body wave function Ψ for N spinless fermions is thus the Slater determinant of these single-particle wave functions occupying $n = 1, 2, \ldots, N$. The density operator can be written as $\hat{\rho} = \sum_i^N \delta(x - x_i)$. Therefore the corresponding density reads,

$$\rho(x) = \langle \Psi | \, \hat{\rho} \, | \Psi \rangle = \sum_n^N \langle \psi_n | \, \delta(x - x_n) \, | \psi_n \rangle = \sum_n^N |\psi_n(x)|^2 = \frac{2}{R} \sum_n^N \sin^2 \left(\frac{n\pi}{R} x \right). \tag{6}$$

In Fig. 7 we show the density profiles of a quantum droplet with $N_A - N_B = 2$ and the sum of the TG density of two particles in a box of size R with the density of the B species. This resulting density has an excellent agreement with the density of the A species.

This feature observed in the density profile enables us to get an approximation of the magnetization for low particle imbalance. To do this, we consider the density of the species A as a sum of the density of B and a density of a Tonks gas of $N_A - N_B$ particles. Thus the mean value of the Tonks density can be written as $\langle \hat{n}_t \rangle = (N_A - N_B)/R$. We can then write,

$$z = \frac{N_A - N_B}{N_A + N_B} = \frac{R \langle \hat{n}_t \rangle}{N_A + N_B} \, . \tag{7}$$

We introduce the expression of the magnetization m_{ab},

$$m_{ab} = \frac{\langle \hat{n}_t \rangle}{2} = \frac{z(N_A + N_B)}{2R} \simeq z n_A \, , \tag{8}$$

where in the last step we do a first approximation to the balanced case $(N_A + N_B)/2 \simeq N_A$ and we write $n_A = N_A/R$. Within this approximation the magnetization is linear in z with a proportionality given by the equilibrium density of the species A. Since the equilibrium density is universal for any number of particles, this approximation of the magnetization is also universal on z. Fig. 6 shows a good agreement of this approximation for low z with numeric results.

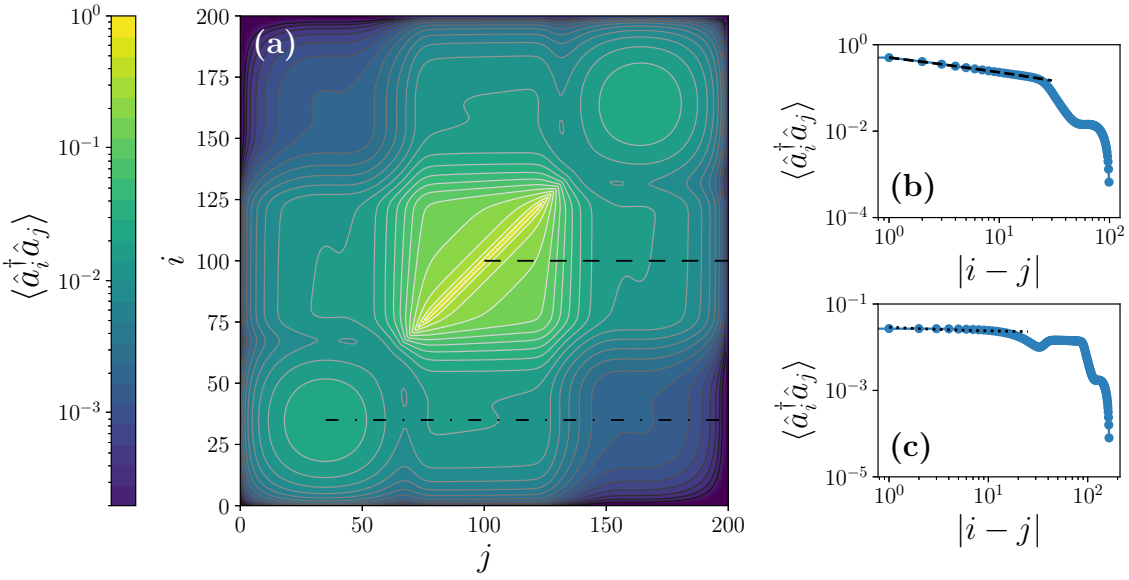

Figure 8: One-body density matrix (OBDM) $\langle \hat{a}_i^\dagger \hat{a}_j \rangle$ where i and j are lattice sites, applied over a quantum droplet that has two expelled particles outside ($N_A = 40$, $N_B = 24$, $U/t = 8$, $r = 0.15$ and $L = 200$). Both panels (b) and (c) are two cuts in which i is fixed and j goes from $j = i$ to $j = L$. In panel (a) we draw these cuts considered for panels (b) and (c) with a dashed and dashed-dotted line, respectively. In panel (b) the dashed line is a fit inside the droplet region with $\langle \hat{a}_i^\dagger \hat{a}_j \rangle \propto 1/|i-j|^\alpha$, where we extract $\alpha \simeq 0.2862$. In panel (c) the dotted line is a fit inside the left gas region with $\langle \hat{a}_i^\dagger \hat{a}_j \rangle \propto 1/\sqrt{|i-j|}$.

4.3 Coherence in quantum droplets

A Bose-Einstein condensate (BEC) created by non-interacting bosons is characterized by the condensation of a large fraction of particles into the lowest single-particle quantum state [DGPS99]. In this situation the presence of BEC is captured by off-diagonal long-range order of the one-body density matrix (OBDM), namely the expectation value $\rho_{ij} = \langle \hat{a}_i^\dagger \hat{a}_j \rangle$ converges to a postive constant for large enough $|i-j|$ [Tas20]. However, in one-dimensional systems strong quantum fluctuations suppress coherence and Bose-Einstein condensation cannot exist [PAG19]. In this situation the OBDM is expected to follow an algebraic decay $\rho_{ij} \propto 1/|i-j|^\alpha$ for sufficiently large $|i-j|$ when a superfluid phase is present.

As we explained in section 2, quantum droplets in the balanced situation can have quasi-long range order, and the coherence is exponentially lost in the Mott Insulator state [MAPJD20].

We now analyze the coherence properties of an imbalanced quantum droplet that has expelled two particles (one in the left and one in the right) studying the OBDM in Fig. 8. The operators $\hat{a}_i$ ($\hat{a}_i^\dagger$) are the annihilation (creation) bosonic operators at site i for the species A, since that is the species that is expelled outside the droplet and we want to consider the coherence between the exterior gas and the droplet. We notice that coherence exists not only inside the droplet but also between droplet and exterior gas. Fig. 8(b) shows the algebraic decay of the OBDM inside the droplet. Outside this one, coherence decays very fast between the droplet and the outside gas. The dashed line in this same panel is a fitting with $\rho_{ij} \propto 1/|i-j|^\alpha$, and we can extract $\alpha \simeq 0.2862$. Fig. 8(c) shows the coherence between the left gas and the rest of the system. We can see that this value is much lower than the results inside the droplet. For the TG regime of a single-component bosonic gas, the OBDM decays with $\rho_{ij} \propto 1/\sqrt{|i-j}$ [Len64]. The dotted line in Fig. 8(c)

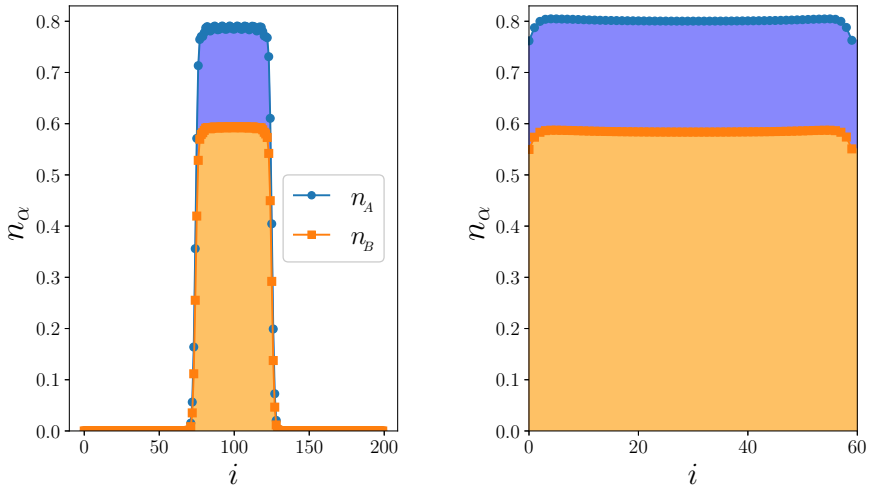

Figure 9: Density profile of both species as a function of the lattice site i for $U/t = 10$ and $r = 0.15$. The left is obtained with open boundary conditions for $N_A = 40$, $N_B = 30$ and $L = 200$. The right is obtained with periodic boundary conditions with a fixed density value that we obtain from the bulk of the left droplet and for a lattice size of $L = 60$.

shows that this function compares well with numeric results in the gas region.

4.4 Thermodynamic limit

In this subsection we study the effect of particle imbalance in thermodynamic solutions. DMRG computations allow to obtain results with periodic boundary conditions. These ones produce a homogeneous solution that for large enough $N = N_A + N_B$ and L we use them as a good approximation to the thermodynamic limit, since it enables us to study the bulk of the droplet without influence from the border of the lattice and the meniscus of the droplet. With this we are able to obtain the equation of state (EOS) for a given interaction U/t, r. We can identify the equilibrium density with the minimum value in the EOS. The spinodal point can also be identified with the point from which the simulations are not stable anymore. This can be identified with an important inhomogeneity in the density profile.

We use these periodic boundary conditions with a fixed density value that we obtain from the bulk of the droplets in open boundary conditions, see Fig. 9. With these homogeneous solutions we are able to compute the chemical potential of the A species,

$$\mu_A = E(N_A, N_B) - E(N_A - 1, N_B)\,, \tag{9}$$

where $E(N_A, N_B)$ is the energy of the homogeneous solution with N_A and N_B particles. In Fig. 10 we show the evolution of the chemical potential of the A species as a function of the imbalance z.

The Bose-Hubbard model of a single species in a one-dimensional lattice with non-interacting particles can be exactly solved. This can be done taking the Bose-Hubbard Hamiltonian with only the tunneling part and doing a discrete Fourier transform on to the momentum space,

$$\hat{H} = -t\sum_j \left(\hat{b}_j^\dagger \hat{b}_{j+1} + \text{h.c.}\right) = -t/N \sum_{q,q'}\sum_{j=1}^{N} \left(e^{-i(qr_j - q'r_{j+1})}\hat{b}_q^\dagger \hat{b}_{q'} + \text{h.c.}\right) \tag{10}$$

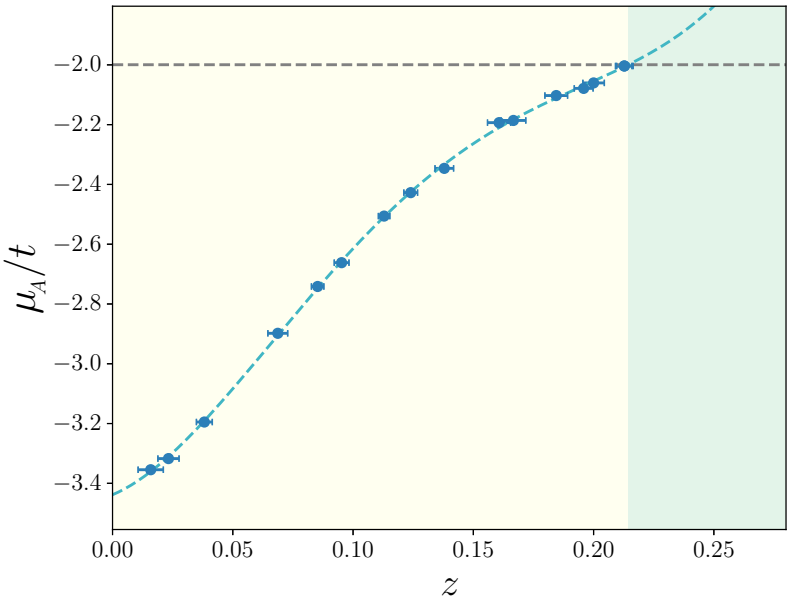

Figure 10: Chemical potential of the A species as a function of the imbalance quantity z. The error bars in the imbalance come from the discretization of the density that is obtained from the simulations in open boundary conditions into a finite simulation in the periodic boundary conditions. The dashed line is a fit with a quartic function. The green background shows the region where the fit is greater than -2. These values are obtained for $U/t = 8$, $r = 0.15$ and $L = 80$.

where N is the number of particles, r_j is the position of the site j, q is the momentum discretized over the first Brillouin zone and we introduced $\hat{b}_i^\dagger = (1/\sqrt{N})\sum_q e^{-iqR_i}\hat{b}_q^\dagger$. We continue,

$$\hat{H} = -t\sum_q \left(e^{iqd} + e^{-iqd}\right)\hat{b}_q^\dagger \hat{b}_{q'} = -2t\sum_q \cos(qd)\hat{b}_q^\dagger \hat{b}_{q'}\,, \tag{11}$$

where from this we can see that the ground state energy of a single particle in a one-dimensional lattice is $-2t$. From this and the computation of the chemical potential μ_A we are able to obtain the expulsion point z^* identifying where $\mu_A > -2t$, since we have seen that is the energy of a free particle in a one-dimensional lattice. This calculation of the expulsion point agrees very well with the calculations performed with open boundary conditions where we can directly identify the expulsion point.

Another procedure we consider to obtain results in the thermodynamic limit is to study the dependence of some quantities with the number of particles $N = N_A + N_B$.

4.5 Bound state insulator

The large bound states we find in the few-body suggest that these may have an important role in the many-body scenario. In the low particle imbalance and large interaction strength situation, we propose that for each B particle removed, a bound state is created. Moreover we interpret that two bound states feel an effective very strong repulsive interaction. This is the case since we have shown that in this region the excess particles formed an effective TG gas on top of the quantum droplet. Thus there is a critical point for increasing particle imbalance where the droplet creates an insulator of these bound states. If we then remove more B particles, the droplet is not able to hold more bound states and thus it will expel A particles. We propose that this is the critical point z^*. Let us consider the size of the

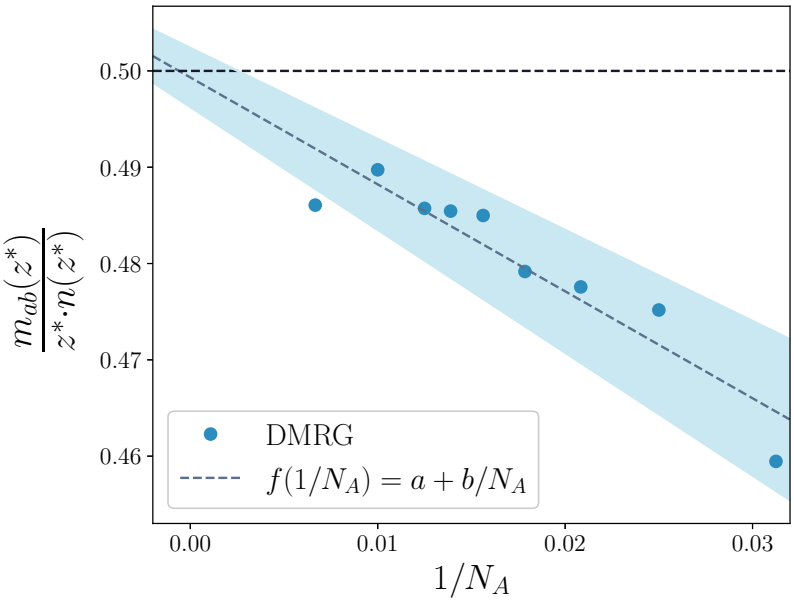

Figure 11: Magnetization divided by the total density $n = n_A + n_B$ and the imbalance quantity z at the last point before particle expulsion, z^*. We fit the obtained values using a function $f(1/N_A) = a + b/N_a$, represented with a grey dashed line in the plot. From this fit we obtain $a = 0.499 \pm 0.03$ and $b = -1.11 \pm 0.17$. The standard deviation of the parameters is displayed with a blue background. This plot is obtained for $U/t = 8$, $r = 0.15$ and we choose L ensuring that the droplets fit inside the lattice.

bound states to be a. When the droplet of size R is fully loaded with bound states thus an insulator is formed. The magnetization m_{ab} will then be,

$$m_{ab}(z^*) = \frac{\langle \hat{n}_A \rangle - \langle \hat{n}_B \rangle}{2} = \frac{\langle \hat{n}_{bs} \rangle}{2} = \frac{1}{2a}\,, \tag{12}$$

where $\langle \hat{n}_{bs} \rangle$ is the averaged density in the bulk of the bound states and in the critical point is equal to $1/a$. We also obtain an expression for the critical point z^*,

$$z^* = \frac{N_A - N_B}{N_A + N_B} = \frac{N_{bs}}{nR} = \frac{1}{na}\,, \tag{13}$$

where N_{bs} is the number of bound states in the droplet of size R and in the last step we have used that $N_{bs} = R/a$. With eq. (12) and (13) we finally obtain,

$$\frac{m_{ab}(z^*)}{z^* \cdot n(z^*)} = \frac{1}{2}\,. \tag{14}$$

This prediction is evaluated in Fig. 11 for different number of particles. If we extrapolate the values to the thermodynamic limit $N \to \infty$ with a function $f(1/N_A) = a + b/N_A$, where a and b are free parameters, the prediction in eq. (14) is compatible with numeric results.

5 Conclusions and outlook

In this work we have studied the effect of particle imbalance in a binary bosonic mixture at zero temperature in a one-dimensional lattice. First, we described the model and reviewed the formation of quantum droplets in the particle-balanced situation, and we introduced key quantities that are studied in this work. We also presented the Density Matrix Renormalization Group (DMRG), the numerical method used to simulate the system and we described the values of the parameters used in the computations.

We presented our results of the effect of particle imbalance in the few- and many-body limits. In the few-body limit, we studied the binding energies of the different bound states, which have shown the formation of large bound states when there is particle imbalance in the system. These larger composites are not found in the balanced situation. We extracted information of these states via the correlation functions and we observed a critical point in which there were not enough B particles to bind the rest A particles. In the many-body regime we introduced the quantity of the magnetization. We add particle imbalance in the system removing the number of B particles and keeping the number of A particles fixed. As this imbalance is increased we identified two different regions: one where droplets gain magnetization and create a droplet with difference in the density of both species and another one where the droplet is not able to support more imbalance, locks the magnetization in the bulk and expels particles outside it for larger values of the particle imbalance. We characterized the coherence between the droplet and the outside gas. The analytical expression of the magnetization presented for low particle imbalance and the relation between the expulsion point and the magnetization show very good agreement with numeric results. We also were able to extract the expulsion point obtaining the chemical potential of the majority component in the mixture with simulations that approximate the thermodynamic limit. We found an excellent agreement between thermodynamic calculations and open-boundary ones.

In Appendix A we studied the convergence of some important quantities in our work with some parameters of DMRG. We detailed the importance of these parameters and we explained the scaling of the computational time with these. The notes presented in this Appendix should be interesting for anybody that wants to simulate such systems with DMRG, since often these numeric details are not explained in literature.

To the best of our knowledge this is the first time that the effect of particle imbalance has been studied on one-dimensional quantum droplets in an optical lattice. We have shown that these are robust against a certain amount of particle imbalance and that they are able to gain magnetization. This feature confirms the viability for an experimental implementation, in which more than often the perfectly balanced situation is difficult to achieve. It would be interesting a more in depth study of the correlations between the gas of expelled particles and the entanglement in the system. In addition, it would also be interesting a study of the effect of the imbalance in the intra-species interaction strength, $U_{AA} \neq U_{BB}$, since that is often the case in experimental setups.

Bibliography

[AM18] GE Astrakharchik and Boris A Malomed. Dynamics of one-dimensional quantum droplets. *Physical Review A*, 98(1):013631, 2018.

[BGH+06] Manuel Barranco, Rafael Guardiola, Susana Hernández, Ricardo Mayol, Jesús Navarro, and Martí Pi. Helium nanodroplets: An overview. *Journal of low temperature physics*, 142(1):1–81, 2006.

[BNSL15] Gergely Barcza, Reinhard M Noack, Jeno Sólyom, and Örs Legeza. Entanglement patterns and generalized correlation functions in quantum many-body systems. *Physical Review B*, 92(12):125140, 2015.

[BSH+20] Fabian Böttcher, Jan-Niklas Schmidt, Jens Hertkorn, Kevin S H Ng, Sean D Graham, Mingyang Guo, Tim Langen, and Tilman Pfau. New states of matter with fine-tuned interactions: quantum droplets and dipolar supersolids. *Reports on Progress in Physics*, 84(1):012403, dec 2020.

[CBP+16] L. Chomaz, S. Baier, D. Petter, M. J. Mark, F. Wächtler, L. Santos, and F. Ferlaino. Quantum-fluctuation-driven crossover from a dilute bose-einstein condensate to a macrodroplet in a dipolar quantum fluid. *Phys. Rev. X*, 6:041039, Nov 2016.

[CCS+18] P. Cheiney, C. R. Cabrera, J. Sanz, B. Naylor, L. Tanzi, and L. Tarruell. Bright soliton to quantum droplet transition in a mixture of bose-einstein condensates. *Phys. Rev. Lett.*, 120:135301, Mar 2018.

[CTS+18] CR Cabrera, L Tanzi, J Sanz, B Naylor, P Thomas, P Cheiney, and L Tarruell. Quantum liquid droplets in a mixture of bose-einstein condensates. *Science*, 359(6373):301–304, 2018.

[DBP+19] C. D'Errico, A. Burchianti, M. Prevedelli, L. Salasnich, F. Ancilotto, M. Modugno, F. Minardi, and C. Fort. Observation of quantum droplets in a heteronuclear bosonic mixture. *Phys. Rev. Research*, 1:033155, Dec 2019.

[DGPS99] Franco Dalfovo, Stefano Giorgini, Lev P Pitaevskii, and Sandro Stringari. Theory of bose-einstein condensation in trapped gases. *Reviews of modern physics*, 71(3):463, 1999.

[FBKS+16] Igor Ferrier-Barbut, Holger Kadau, Matthias Schmitt, Matthias Wenzel, and Tilman Pfau. Observation of quantum droplets in a strongly dipolar bose gas. *Phys. Rev. Lett.*, 116:215301, May 2016.

[GAB+20] G. Guijarro, G. E. Astrakharchik, J. Boronat, B. Bazak, and D. S. Petrov. Few-body bound states of two-dimensional bosons. *Phys. Rev. A*, 101:041602, Apr 2020.

[Gir60] Marvin Girardeau. Relationship between systems of impenetrable bosons and fermions in one dimension. *Journal of Mathematical Physics*, 1(6):516–523, 1960.

[Has07] M B Hastings. An area law for one-dimensional quantum systems. *Journal of Statistical Mechanics: Theory and Experiment*, 2007(08):P08024–P08024, aug 2007.

[HMD+09] Anzi Hu, L. Mathey, Ippei Danshita, Eite Tiesinga, Carl J. Williams, and Charles W. Clark. Counterflow and paired superfluidity in one-dimensional bose mixtures in optical lattices. *Phys. Rev. A*, 80:023619, Aug 2009.

[HMSW15] Claudius Hubig, Ian P McCulloch, Ulrich Schollwöck, and F Alexander Wolf. Strictly single-site dmrg algorithm with subspace expansion. *Physical Review B*, 91(15):155115, 2015.

[HP18] Johannes Hauschild and Frank Pollmann. Efficient numerical simulations with Tensor Networks: Tensor Network Python (TeNPy). *SciPost Phys. Lect. Notes*, page 5, 2018.

[Kru16] Konstantin V Krutitsky. Ultracold bosons with short-range interaction in regular optical lattices. *Physics Reports*, 607:1–101, 2016.

[Lan50] Cornelius Lanczos. An iteration method for the solution of the eigenvalue problem of linear differential and integral operators. 1950.

[Len64] Andrew Lenard. Momentum distribution in the ground state of the one-dimensional system of impenetrable bosons. *Journal of Mathematical Physics*, 5(7):930–943, 1964.

[LSA12] Maciej Lewenstein, Anna Sanpera, and Veronica Ahufinger. *Ultracold Atoms in Optical Lattices: Simulating quantum many-body systems*. OUP Oxford, 2012.

[MAPJD20] Ivan Morera, Grigori E Astrakharchik, Artur Polls, and Bruno Juliá-Díaz. Quantum droplets of bosonic mixtures in a one-dimensional optical lattice. *Physical Review Research*, 2(2):022008, 2020.

[MAPJD21] Ivan Morera, Grigori E. Astrakharchik, Artur Polls, and Bruno Juliá-Díaz. Universal dimerized quantum droplets in a one-dimensional lattice. *Phys. Rev. Lett.*, 126:023001, Jan 2021.

[Or4] Román Orús. A practical introduction to tensor networks: Matrix product states and projected entangled pair states. *Annals of Physics*, 349:117–158, 2014.

[PA16] D. S. Petrov and G. E. Astrakharchik. Ultradilute low-dimensional liquids. *Phys. Rev. Lett.*, 117:100401, Sep 2016.

[PAG19] L Parisi, GE Astrakharchik, and Stefano Giorgini. Liquid state of one-dimensional bose mixtures: a quantum monte carlo study. *Physical review letters*, 122(10):105302, 2019.

[Pet15] D. S. Petrov. Quantum mechanical stabilization of a collapsing bose-bose mixture. *Phys. Rev. Lett.*, 115:155302, Oct 2015.

[SC95] Jun John Sakurai and Eugene D Commins. Modern quantum mechanics, revised edition, 1995.

[Sch11] Ulrich Schollwöck. The density-matrix renormalization group in the age of matrix product states. *Annals of Physics*, 326(1):96–192, 2011. January 2011 Special Issue.

[SFM+18] G. Semeghini, G. Ferioli, L. Masi, C. Mazzinghi, L. Wolswijk, F. Minardi, M. Modugno, G. Modugno, M. Inguscio, and M. Fattori. Self-bound quantum droplets of atomic mixtures in free space. *Phys. Rev. Lett.*, 120:235301, Jun 2018.

[SGM19] Tomasz Sowiński and Miguel Ángel García-March. One-dimensional mixtures of several ultracold atoms: a review. *Reports on Progress in Physics*, 82(10):104401, 2019.

[SM98] D W L Sprung and J Martorell. The symmetrized Fermi function and its transforms. *Journal of Physics A: Mathematical and General*, 31(44):8973–8975, nov 1998.

[SWB+16] Matthias Schmitt, Matthias Wenzel, Fabian Böttcher, Igor Ferrier-Barbut, and Tilman Pfau. Self-bound droplets of a dilute magnetic quantum liquid. *Nature*, 539(7628):259–262, 2016.

[Tas20] Hal Tasaki. *Physics and mathematics of quantum many-body systems*, volume 62. Springer, 2020.

[TOH+04] B Laburthe Tolra, KM O'hara, JH Huckans, William D Phillips, SL Rolston, and James V Porto. Observation of reduced three-body recombination in a correlated 1d degenerate bose gas. *Physical review letters*, 92(19):190401, 2004.

[Whi92] Steven R. White. Density matrix formulation for quantum renormalization groups. *Phys. Rev. Lett.*, 69:2863–2866, Nov 1992.

A DMRG Convergence

In order to obtain the ground state of the system we employ the Density Matrix Renormalization Group (DMRG) algorithm. This allows us to obtain the ground state of the system given a number of particles and a system size. At the same time, DMRG sets a number of variational parameters set by the bond dimension χ and the dimension of the local Hilbert space d. To properly obtain reliable physical results we study how the ground state properties depend on the number of variational parameters. At the same time, our limited classical computational resources force us to reduce the size of the simulations in order to be able to compute them in feasible time. This balance between these two constrains is what we study in this Appendix.

In each sweep of the DMRG algorithm we apply an effective Hamiltonian over the Matrix Product State (MPS) updating consecutively one (single-site DMRG) or two sites (two-site DMRG) in order to minimize the energy [HMSW15]. DMRG computations have been performed using TeNPy [HP18]. This one uses the two-site DMRG and thus we focus only on this algorithm in the following. The effective Hamiltonian can be written as a matrix of dimensions $\chi_{\text{max}}^2 d^2 \times \chi_{\text{max}}^2 d^2$ [HP18], where χ_{max} is the maximum bond dimension in the two-sites updated and d is the dimension of the Hamiltonian in a single-site. The most computationally expensive part of DMRG is to minimize the energy when the effective Hamiltonian is applied. To do this, we use the Lanczos algorithm [Lan50], which typically converges after a few tensor products that scale $\mathcal{O}\left(\chi_{\text{max}}^3 D d^2 + \chi_{\text{max}}^2 D^2 d^3\right)$, where D is the bond dimension of the Hamiltonian written as a Matrix Product Operator (MPO).

The convergence criteria to stop DMRG sweeps is when the relative change in the energy at each tensor update in a sweep is $\Delta E/|E| < -10^{-8}$ and the entropy $\Delta S/S < 10^{-5}$.

The computations used in this work have been produced by three different computers. Two of these are desktop computers and the third is a cluster of central processing units (CPU's). We want to thank Dr. Arnau Rios for letting us access into this computer cluster. In Table 1 we detail the main hardware specifications of these three computers.

Computer	CPU model	Number of CPU's	RAM memory
Desktop computer #1	Intel® Core™ i5-8400 CPU - 2.80 GHz	6	49.321 GB
Desktop computer #2	Intel® Core™ i5-4430 CPU - 3.00GHz	4	16.456 GB
CPU Cluster	Intel® Xeon® Gold 6240R CPU - 2.40 GHz	96	202.35 GB

Table 1: Hardware specifications of the different computers used in this work.

TeNPy allows to parallelize the code to run in multiple CPU's. This feature would enable us to take advantage of the vast number of CPU that the cluster has. Nevertheless we have seen that the optimal number of CPU's in TeNPy are $2-3$. Since in this work we focus on the effect of particle imbalance, we need to compute a large number of simulations for different number of particles between both species. Therefore we use our computers to simulate a great number of these simulations at once which use $2-3$ CPU's each.

Another added benefit from working in a CPU cluster is the total RAM size. As an example, a simulation of a droplet with maximum bond dimension $\chi = 4096$ occupies

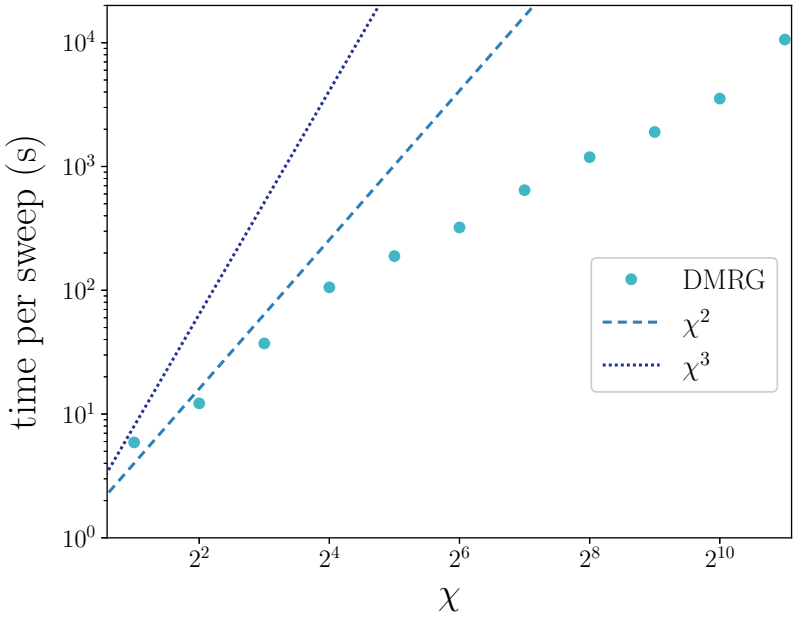

Figure 12: Time of computation of one DMRG sweep as a function of the maximum bond dimension χ. In a dashed and a dotted line, the functions χ^2 and χ^3, respectively. This DMRG computation is for $N_A = 40$, $N_B = 36$, $U/t = 8$, $r = 0.15$, $L = 100$ and $M = 4$.

approximately 50 gigabytes of RAM memory. In both desktop computers the RAM memory is inferior to this number. Thus we would only be able to compute this simulation using the cluster.

Since we have an important but finite computing resources available, a crucial duty is to minimize the size and total time of computations by reducing key parameters in DMRG. This has to be done carefully to obtain meaningful results. In the following subsections we explain our criteria in choosing two of these parameters: the bond dimension and the maximum number of bosons per site.

A.1 Bond dimension

The bond dimension in a MPS is the dimension of the bond index that connects two following tensors. This quantity can give a measure of the amount of entanglement in the wave function [Or4]. As we explained, the most computational expensive part of DMRG scales as $\mathcal{O}\left(\chi_{\max}^3 D d^2 + \chi_{\max}^2 D^2 d^3\right)$. Therefore in DMRG we have to limit the bond dimension up to a predefined value χ to perform the simulations in a realistic time. In Fig. 12 we show the scaling of the computational time with the bond dimension. Surprisingly, this one scales with an exponent of χ smaller than the prediction $\mathcal{O}\left(\chi_{\max}^3 D d^2 + \chi_{\max}^2 D^2 d^3\right)$ given in [HP18].

The convergence of the quantities used in this work has to be carefully studied since the value of χ can have an important role in the results of the simulations. In Fig. 13 we report the convergence of different quantities for a particle-imbalanced droplet with different maximum bond dimension χ. We are able to obtain a prediction to the limit of $\chi \to \infty$ with a fit of the results to a function of $1/\chi$. In our work a crucial quantity is the magnetization m_{ab}. For $\chi = 256$ the error in the magnetization is on the forth decimal. We consider that this error is small enough and we choose this value for simulations in which we want to obtain m_{ab}.

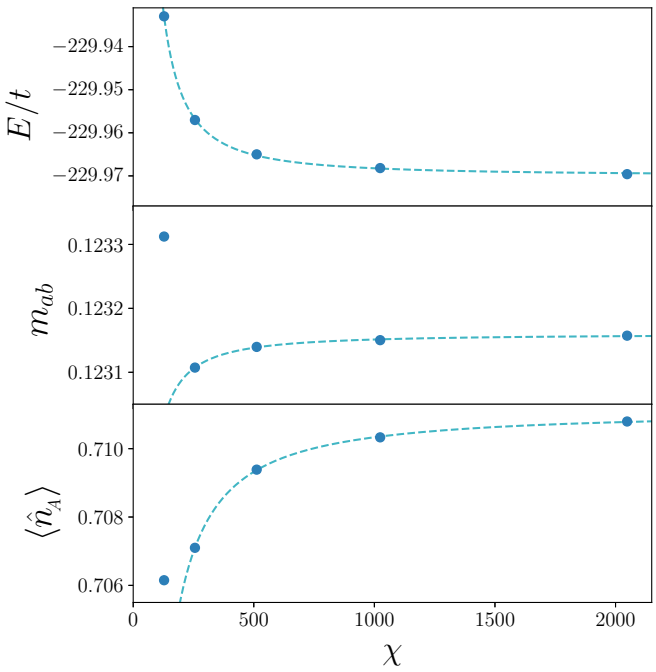

Figure 13: Convergence of different quantities as a function of the maximum bond dimension, χ. We fit each quantity with a function $f(\chi) = a + b/\chi^c$, where a, b and c are free parameters. In the second and third panel we exclude the first value to do the fit. Values obtained with a particle-imbalanced droplet for $N_A = 40$, $N_B = 24$, $U/t = 8$, $r = 0.15$, $L = 144$ and $M = 4$.

Although $\chi = 256$ is enough for the mentioned quantities we also show that it is not sufficient for more complex quantities. In particular, correlation functions measure the correlation between different parts of the system and thus are quantities highly influenced by the entanglement [BNSL15]. This means that these functions have harder convergence on the bond dimension χ. In addition, a limit in the bond dimension is translated into a limit in the entanglement of the system. Thus we expect correlation between long distances to need a relatively large χ to converge. In Fig. 14 we present the evolution of the one-body density matrix (OBDM) $\langle \hat{a}_i^\dagger \hat{a}_j \rangle$ as a function of $|i - j|$ for a particle-imbalanced droplet that has expelled two particles (one in each side of the droplet). The operators $\hat{a}_i$ ($\hat{a}_i^\dagger$) are the annihilation (creation) bosonic operators at site i for the species A. In Fig. 14(b) we show the OBDM for large values of $|i - j|$ and it can clearly be seen that higher values of the bond dimension are needed in order to accurately obtain the quantity in this region. Since we have a somewhat limited amount of computing power, we are only able to work up to $\chi = 2048$ and we use this value for the OBDM results in our work.

A.2 Maximum number of bosons per site

Our system consists of a one-dimensional lattice with N_A and N_B atoms of A and B particles, respectively. Thus we can have from 0 to $N_A + N_B$ atoms in each lattice site. This means that the dimension d of the effective Hamiltonian in one site is $d = (N_A + 1)(N_B + 1)$. Although this would be the exact way to proceed, it is not computationally feasible since the dimension of the local Hamiltonian would be too large. Therefore we put a cutoff on the maximum number of bosons of each species per site M. This sets a maximum dimension of the local Hamiltonian. In this subsection we study how this value affects the density profiles and the energy of the system.

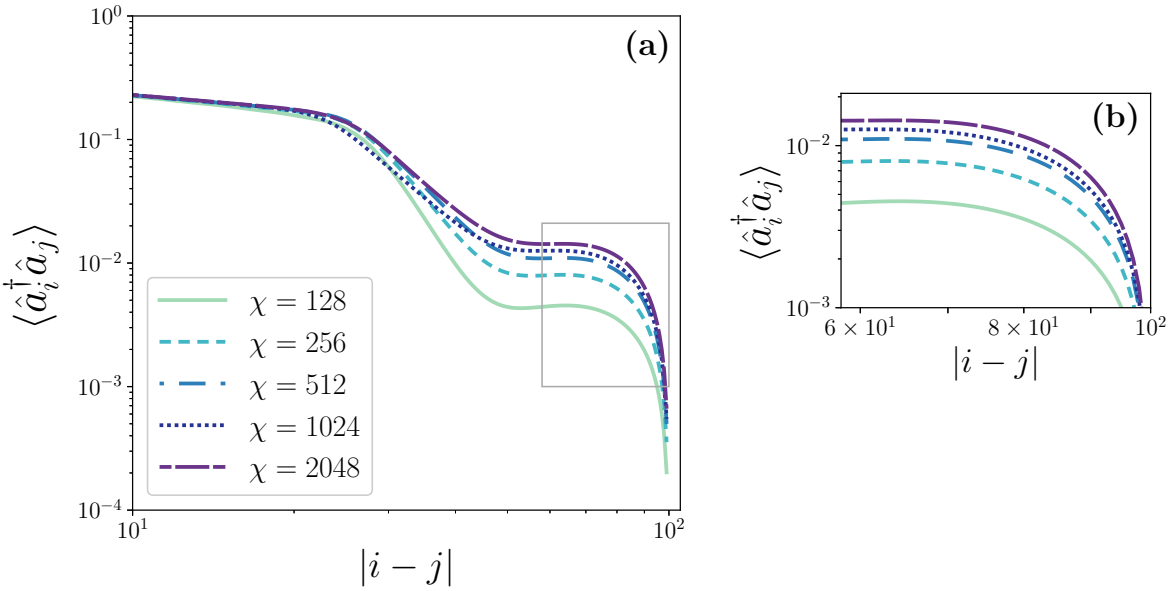

Figure 14: One-body density matrix $\langle \hat{a}_i^\dagger \hat{a}_j \rangle$ with i fixed on the middle of the lattice and j scans from $j = i$ to the end of the lattice. In panel (b) we enlarge the gray area marked in panel (a). Values obtained with a particle-imbalanced droplet for $N_A = 40$, $N_B = 24$, $U/t = 8$, $r = 0.15$, $L = 144$ and $M = 4$.

Before introducing imbalance, we study the effect of the cutoff M in the balanced situation $N_A = N_B$. In Fig. 15 the mean density of the bulk of a droplet for the balanced situation as a function of the interaction strength U/t is reported. We choose $M = 4$ as the value used for computations in our work since it already shows a good convergence in the averaged density. Moreover, in our work we focus on the strongly interacting regime, that is the region of sufficiently large U/t, which is also the region where the convergence in M much is faster.

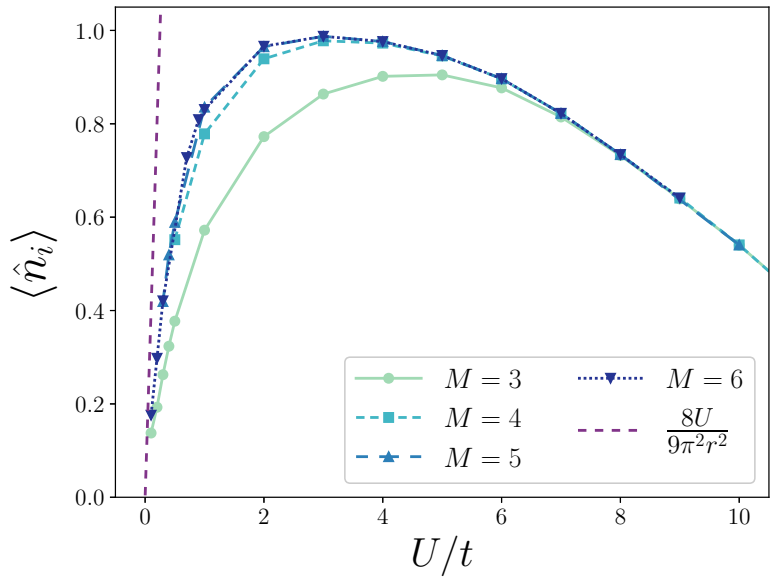

Figure 15: Averaged central density in the bulk of the droplet as a function of the interaction strength U/t for $r = 0.15$ and different L, ensuring that the droplets fit inside the lattice.

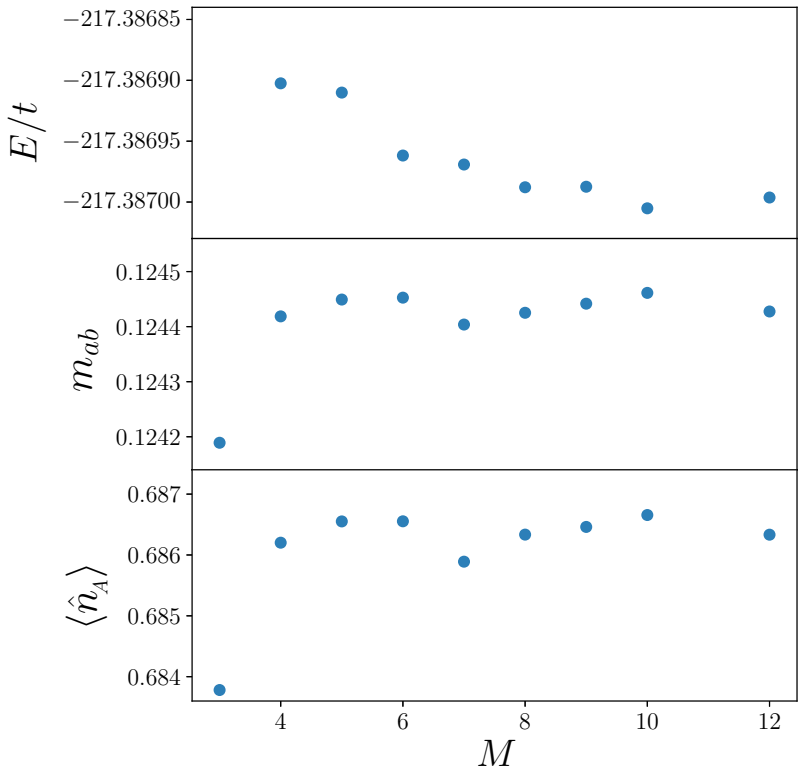

Figure 16: Convergence of different quantities as a function of the cutoff of maximum number of bosons of each species per site, M. Values obtained with a particle-imbalanced droplet for $N_A = 40$, $N_B = 22$, $U/t = 8$, $r = 0.15$, $L = 144$ and $\chi = 256$.

Now we consider a system with particle imbalance and we study the effect of the value M. In Fig. 16 the convergence of some quantities for different values of M is shown. For $M \leq 4$ the magnetization and density oscillates between the forth and third decimal, respectively. The energy difference for $M > 4$ is on the fifth decimal, a value that is equivalent to the convergence criteria of DMRG. Therefore we conclude that for the range of $U/t \in (8, 10)$, $M = 4$ is a sufficient value to obtain valid results.